HHS Public Access

Author manuscript

Nanotoxicology. Author manuscript; available in PMC 2016 September 22.

Published in final edited form as:

Nanotoxicology. 2016 ; 10(1): 118–127. doi:10.3109/17435390.2015.1038330.

Low-dose AgNPs reduce lung mechanical function and innate immune defense in the absence of cellular toxicity

Danielle J. Botelho[1], **Bey Fen Leo**[2,3], **Christopher B. Massa**[1], **Srijata Sarkar**[4], **Terry D. Tetley**[5], **Kian Fan Chung**[5], **Shu Chen**[2], **Mary P. Ryan**[2], **Alexandra E. Porter**[2], **Junfeng Zhang**[6], **Stephan K. Schwander**[4], and **Andrew J. Gow**[1]

[1]Department of Pharmacology & Toxicology, Rutgers University, Piscataway, NJ, USA

[2]Department of Materials and London Centre for Nanotechnology, Imperial College London, London, UK

[3]Department of Mechanical Engineering, University of Malaya, Kuala Lumpur, Malaysia

[4]School of Public Health, Rutgers University Piscataway, NJ, USA

[5]National Heart and Lung Institute, Imperial College London, London, UK

[6]Department of Preventive Medicine, University of Southern California (currently Duke University), Durham, NC, USA

Abstract

Multiple studies have examined the direct cellular toxicity of silver nanoparticles (AgNPs). However, the lung is a complex biological system with multiple cell types and a lipid-rich surface fluid; therefore, organ level responses may not depend on direct cellular toxicity. We hypothesized that interaction with the lung lining is a critical determinant of organ level responses. Here, we have examined the effects of low dose intratracheal instillation of AgNPs (0.05 μg/g body weight) 20 and 110nm diameter in size, and functionalized with citrate or polyvinylpyrrolidone. Both size and functionalization were significant factors in particle aggregation and lipid interaction *in vitro*. One day post-intratracheal instillation lung function was assessed, and bronchoalveolar lavage (BAL) and lung tissue collected. There were no signs of overt inflammation. There was no change in surfactant protein-B content in the BAL but there was loss of surfactant protein-D with polyvinylpyrrolidone (PVP)-stabilized particles. Mechanical impedance data demonstrated a significant increase in pulmonary elastance as compared to control, greatest with 110nm PVP-stabilized particles. Seven days post-instillation of PVP-stabilized particles increased BAL cell counts, and reduced lung function was observed. These changes resolved by 21 days. Hence, AgNP-mediated alterations in the lung lining and mechanical function resolve by 21 days. Larger particles and PVP stabilization produce the largest disruptions. These studies demonstrate that low dose AgNPs elicit deficits in both mechanical and innate immune defense function, suggesting that organ level toxicity should be considered.

Correspondence: Andrew Gow, Ernest Mario School of Pharmacy, Rutgers University, 160 Frelinghuysen Road, Piscataway, NJ 08854, USA., Tel: +1 8484454613. gow@rci.rutgers.edu.

Supplementary material available online

Supplementary Figures S1–S11

Keywords

Bronchoalveolar lavage fluid; inflammation; polyvinylpyrrolidone; pulmonary function; surfactant

Introduction

Engineered silver nanoparticles (AgNPs) have many uses, and are in high demand for their antimicrobial properties. Industrial AgNPs are used in air purifiers, water purifiers, washing machines and as a component for inks used in inkjet printers (Clement & Jarrett, 1994; Shim et al., 2008; Tolaymat et al., 2010). As the commercial use of AgNPs has grown, multiple studies have been aimed at determining the toxic effects arising from high doses of AgNPs and their interactions within different organ systems. The respiratory system is a primary target for exposure (Bakshi et al., 2008). Although numerous studies have examined particle–particle interactions in various media and particle–surfactant interactions *in vitro* and *in vivo* (Dhar et al., 2012; Foldbjerg et al., 2011; Leo et al., 2013; Salvador-Morales et al., 2007; Tatur & Badia, 2012), potential effects on the organ-level physiology and toxicity at low doses of AgNPs are still poorly understood and these doses may more accurately reflect real world exposure.

Surface chemistry and particle size are key factors that determine nanoparticle interactions within a biological system (Mu et al., 2014; Shang et al., 2014). These factors determine redox potential, particle–particle interaction, particle–protein interaction, particle–lipid interaction, deposition of particles and cellular clearance of particles (Mu et al., 2014). During the synthesis process, AgNPs are often stabilized by a “capping agent” such as citrate and polyvinylpyrrolidone (PVP). PVP binds to the core of AgNPs by steric interaction producing a stronger association than citrate which binds AgNPs via ionic interactions. PVP-stabilized particles do not readily aggregate or precipitate out of culture media. In contrast, citrate-stabilized particles can rapidly aggregate and precipitate when suspended in high ionic strength buffers due to charge screening effects. How these different stabilization mechanisms affect AgNP interactions with the lung lining fluid is currently unknown.

Nanoparticles are readily deposited in the lower airways of the lung, and the lung lining fluid is a highly absorptive layer, which can absorb those particles. *In vitro* studies have already shown that nanoscale particles can become coated by the lipid portion of the lung lining fluid causing the particles to form strands in a manner dependent upon surfactant protein B (SP-B). This interaction leads to an increase in surface tension and a decrease in the absorptive properties of the synthetic lipid layer *in vitro* (Bakshi et al., 2008). It has also been shown that surfactant proteins A and D (SP-A&D) bind to functionalized carbon nanotubes in a calcium-dependent manner (Salvador-Morales et al., 2007). SP-A&D, often termed collectins, are key regulators of the innate immune system within the lung. It is reasonable to postulate that collectin association to NPs may facilitate phagocytosis and clearance of these particles by the cells of the lung lining (Ruge et al., 2012). However, such binding may also affect surfactant recycling and/or secretion by the Type II alveolar cells (Salvador-Morales et al., 2007). Hence, we hypothesize that AgNPs potentially disrupt

pulmonary physiology by altering respiratory function (by altering the biophysical properties of surfactant), immune defense (by altering innate immune regulation) and the homeostatic regulation of surfactant protein levels.

The aim of this study is to measure the effects of size and surface chemistry of AgNPs at an acute, low particle dose (below the level of cellular toxicity) upon lung mechanical function and biochemistry. A low dose of AgNPs was used to reduce possible injury and inflammation, and allow for determination of the relationship between particle biophysics and lung function. We used the following four different types of AgNPs with combinations of two diameters (20 nm vs. 110 nm) and two capping agents (citrate and PVP). The interaction between each type of AgNP and a model surfactant was measured *in vitro*; while markers of inflammation and injury were examined 24 h post-intratracheal instillation using histology, cell counts and differentials, real-time polymerase chain reactions (RT-PCR), immunoblotting for SP-B and SP-D, capillary surfactometry and mechanical ventilation with forced oscillation maneuvers to measure impedance. Persistence of AgNP mediated changes were also analyzed at 7 and 21 days post-instillation. These studies examine how the characteristics of size and functionalization alter the ability of AgNPs to disrupt lung mechanical function and innate immune defense in the absence of overt inflammation.

Methods

Silver nanospheres

All four types of AgNPs were manufactured by nanoComposix, Inc. (San Diego, CA) via base-catalyzed reduction of silver nitrate using 5–7 nm gold seed as nucleation centers. The size of the particles was measured by the Nanotechnology Characterization Laboratory, National Cancer Institute at Frederick using TEM and ICP-MS. The AgNPs were subsequently provided by the Consortium of NIEHS Centers for Nanotechnology Health Implications Research (NCNHIR). The particles were further characterized, using TEM, energy dispersive X-ray spectroscopy (EDX) and zeta potential measurements. AgNPs (110 nm) were further characterized using high angle annular dark field scanning transmission electron microscopy (HAADF-STEM). HAADFSTEM combined with EDX analysis was carried out using an FEI Titan 80/300 fitted with a Cs (image) corrector, monochromator and EDX detector (EDAX, Leicester, UK) operated at an accelerating voltage of 80 kV. For STEM experiments, a convergence semi-angle of 14 mrad was used, with an inner and outer HAADF collection angle of 49 and 239 mrad, respectively. The probe diameter was <0.5 nm.

Stability of AgNPs: dissolution kinetics

Aliquots of Ag solutions were taken for inductively coupled plasma-optical emission spectroscopy (ICP-OES) analysis at various time points from 1 h up to 3 days (72 h). ICP-OES was used to determine the amount of dissolved Ag at pH 5 and 7. To minimize the impact of anions on the stability of the AgNPs, non-interacting buffers were used and perchloric acid (Sigma-Aldrich, St. Louis, MO) was used to adjust the pH. Each AgNP suspension (PVP or citrate coating) was incubated in a temperature controller at 37 °C and then centrifuged at high speed (13 000 rpm) with 2 kDa (<4 nm) filter tubes (Sartorius

Stedim VIVACON 500, Goettingen, Germany) to separate any NPs from the solution. For the control experiment, deionized water (no AgNPs) and supernatant from which the AgNPs had been removed were analyzed to ensure that any residual AgNPs were removed during centrifugation and filtering.

Stability of AgNPs: morphology evolution

TEM was performed using a JEOL 2010 instrument (Tokyo, Japan) operated at an accelerating voltage of 200 kV. The effect of pH, particle size and surface chemistry on the stability of AgNPs (25 mg L^{-1}) was studied in the presence and absence of dipalmitoylphosphatidylcholine (DPPC). This assay was designed to examine lipid–AgNP interactions, not to model the alveolar environment where interactions are complicated by the presence of surfactant proteins (Tatur & Badia, 2012). DPPC solutions of 100 mg L^{-1} were prepared in perchlorate acid solutions (pH 5) by sonication for 10 min using an ultrasonic bath. The samples were incubated at 37 °C for 1 day (24 h) in a dri-block heater. TEM samples were prepared by depositing a single drop of the suspension on a 300 Cu Mesh holey support film and were left to dry at room temperature and stored under vacuum.

Murine model and particle instillation

Nine-week-old C57-BL6 Jackson wild-type male mice were intratracheally instilled with AgNPs, or water (50 μl) for control, following anesthesia using a ketamine/xylazine combination. Particles, at 0.05 μg AgNP/g body weight, were suspended into water to a final volume of 50 μl. Citrate-stabilized particles can rapidly aggregate and precipitate in high ionic strength buffers (Tejamaya et al., 2012). Therefore, AgNPs were suspended in a non-ionic solution (water), at a low dose. Particles were mixed in solution using probe sonication immediately before intratracheal instillation. To determine a particle dose that was sub-toxic, as defined by a failure to increase lung leak 24 h post-administration, mice were instilled with 0.05, 0.15, 0.45 or 1.35 μg AgNP/g body weight. At 24 h post-instillation animals were injected with Evan's Blue Dye retro-orbitally. Lungs were lavaged and dye content was measured spectrophotometrically. A dose of 0.05 μg AgNP/g body showed no significant increase in dye content. Mice were left for 1, 7 or 21 days before being anesthetized and mechanical function assessed (see below). Following lung function assessment (described below), the mice were exsanguinated and tissues were harvested and analyzed as described below.

This protocol was approved by the Rutgers University Institutional Animal Care and Use Committee (IACUC) (Protocol Number: 06-028). The study was conducted in accordance with the recommendations in the Guide for the Care and Use of Laboratory Animals of the National Institutes of Health. Intratracheal instillations and mechanical ventilation were conducted under ketamine/xylazine anesthesia, and all efforts were made to minimize suffering. Animals were sacrificed using a lethal dose of ketmine/xylazine and exsanguination.

Bronchoalveolar lavage

The whole lung of each mouse was lavaged (prior to inflation fixing with paraformaldehyde) with 10mM HEPES buffered saline in 1mL increments four times. Cells from the

bronchoalveolar lavage (BAL) were then centrifuged (300 *g*, 10 min). The supernatant was collected for protein and lipid analysis. The cell pellet was re-suspended in 1mL buffered saline for cytology and RT-PCR (Atochina-Vasserman et al., 2009; Casey et al., 2005; Groves et al., 2012).

Histology

The left lung was harvested and inflation fixed using a 3% paraformaldehyde in 2% sucrose solution. Lungs were then embedded in paraffin, sectioned and stained with hematoxylin and eosin (H&E). Lung images were captured using the Olympus VS120-SL Virtual Slide System (Shinjuku, Tokyo, Japan) (Atochina-Vasserman et al., 2009; Groves et al., 2012).

Cell counts and cytology

Cell number was assessed using a Beckman Coulter Multisizer™ 3 Coulter Counter® (Brea, CA). Approximately 30 000 cells were then centrifuged onto a glass slide at 800 *g* for 3 min, air dried, and then stained with Diff-Quik buffered modified Wright-Giemsa stain. Cell differentials were performed manually using a light microscope at 40× magnification (Atochina-Vasserman et al., 2009; Casey et al., 2005; Groves et al., 2012).

Lactate dehydrogenase activity assay

A lactate dehydrogenase (LDH) assay was performed using BAL fluid to assess general cellular cytotoxicity. Chemicals and protocol were used from an *In Vitro* Toxicology Assay Kit, Lactic Dehydrogenase based by Sigma-Aldrich® (Demokritou et al., 2013; Warheit et al., 2013).

Real-time polymerase chain reactions

RNA was prepared from BAL cells using a QIAGEN® QIAshredder™ kit (Venlo, Limburg, Netherlands) and converted to cDNA. The cell samples for each treatment group were pooled into one larger sample for analysis. Thermocycling was used to analyze mRNA expression of CCL2 (mCCL2 1F103: CCT GCT GCT ACT CAT TCA CCA; mCCL2 1R259: GTC TGG ACC CAT TCC TTC TTG), IL1B (mIL1b1F216: TGT GGC AGC TAC CTG TGT CTT; mIL1b1R321: TCC CAT GAG TCA CAG AGG ATG), IL6 (mIL6F23: GAC TTC CAT CCA GTT GCC TTC; mIL6R125: TGG GAG TGG TAT CCT CTG TGA), CXCL10 (mCXCL10F12: AGT GCT GCC GTC ATT TTC TGC; mCXCL10R139: CCT ATG GCC CTC ATT CTC ACT) and IL12B (mIL12bF131: GTG ACA CGC CTG AAG AAG ATG; mIL12bR303: CTT CTT GTG GAG CAG CAG ATG). The ABI 7900HT Fast Real-Time PCR System by Applied Biosystems (Waltham, MA) was used and primers were designed with OligoPerfect™ Designer (lifetechnologies.com, Carlsbad, CA). Fold expression was calculated by the ΔΔCT method normalizing to the water (control) treatment group and using actin as the control gene (Sarkar et al., 2012).

Immunohistochemistry

To qualitatively assess cellular recruitment in response to AgNP treatment and better define the macrophage population within the lung, paraffin-embedded tissue sections were stained

using an antibody for Cd11b (ab133357, anti-rabbit, abcam®, Cambridge, MA). Cd11b serves as a marker for recruited monocytes (Dhaliwal et al., 2012; Ding et al., 2011).

Protein and phospholipid assay

Whole BAL protein concentration was determined using a Low Protein BCA Assay kit by Lamda Biotech, Inc. (St. Louis, MO). To estimate phospholipid content, whole BAL was fractionated into small and large aggregate portions by centrifugation at 17 000*g* for 1 h at 4 °C. The supernatant was the protein-rich small aggregate fraction. The pellet was re-suspended in a small volume of saline (35 μl) and was the lipid-rich large aggregate fraction. Inorganic phosphate from the lipid-rich fractions was measured as an estimate of the phospholipid content (Atochina-Vasserman et al., 2009; Bligh & Dyer, 1959).

Immunoblotting

To determine surfactant protein content, reducing NuPAGE was performed using individual BAL samples. Gels were transferred to BioRad Immun-blot® PDVF membranes, incubated with SP-D or SP-B antibody (M.F. Beers, University of Pennsylvania), goat-α-rabbit linked to horseradish peroxidase, and imaged using Amersham™ ECL™ Prime Western Blotting Detection Reagent (Buckinghamshire, United Kingdom). Densitometry was performed to quantify the chemiluminescent signal. Whole BAL was used for SP-D analysis; and sample load was normalized to protein concentration. Large aggregate BAL (LA BAL) was used for SP-B analysis and sample load was normalized to phospholipid content as determined by the phospholipid assay (Atochina-Vasserman et al., 2009).

Capillary surfactometry

Surface tension was measured using a capillary surfactometer (Calmia Medical, Inc., Toronto, Ontario, Canada). Samples were loaded at a consistent phospholipid concentration of 1.0 μg/μl. Following sample loading, compressed air was applied to the capillary at increasing pressures. Both the initial pressure to disrupt the LA BAL and percent capillary open over the course of 2 min were recorded (Atochina-Vasserman et al., 2009).

Mechanical ventilation and respiratory model

Mice were anesthetized and ventilated using the flexiVent (SCIREQ, Montreal, Canada) at increasing positive end expiratory pressures (PEEPs) (0, 1, 3 and 6 cm H_2O) to assay for resolution of lung function (Allen & Bates, 2004). Mechanical ventilation with forced oscillation maneuvers was used to measure impedance broadband signal (0.5–20 Hz) respiratory impedance [Z(f)] (Moriya et al., 2003). The flow [$V(t)$] is a known value input into the system, while pressure [$P(t)$] output is unknown. As mechanical function varies with frequency of oscillation, a Fourier transform was performed so that impedance could be expressed as a function of frequency, $Z(f) = P(f)/V(f)$. Output impedance spectra were used to generate resistance (R_L) and elastance (E_L) spectra across the frequency range, and fit to a model of heterogeneous lung function using the following equations (Groves et al., 2012, 2013; Massa et al., 2014):

$$R_L = \frac{a+bf}{c+f} \text{ and } E_L = E_0 + \Delta E(1 - e^{-\beta f}). \quad (1)$$

Statistical analysis

All data (excluding respiratory mechanics) were analyzed using one-way ANOVA and the Holm-Sidak method, a p value of <0.05 was considered statistically significant. In the case of respiratory modeling, model fits were estimated for each treatment group by fitting a non-linear regression curve to the spectra of all mice in a treatment group equally at each PEEP. Spectra were analyzed for significant differences using the null hypothesis that the data can be characterized by one three-parameter relationship or alternatively that the data are distinct enough to be characterized by two three-parameter relationships. The parameters of the R_L and E_L curves were estimated from non-linear regressions fitting to the spectra of each individual mouse within a treatment group at each PEEP. Then, a mean and standard error for each parameter was taken for each treatment group (Groves et al., 2013; Massa et al., 2014). A one-way ANOVA was used to determine significant differences in the mean value of each parameter for treatment groups and PEEP. Pair-wise comparisons were made using the Holm-Sidak method.

Results

Particle characterization

In-house characterization analysis confirmed that as-received AgNPs had the physicochemical properties as shown in Figure S1; the zeta potentials are more similar than would be expected (the citrate capping may have surface-exchanged reducing the effective charge for these particles): all show a negative potential consistent with manufacturers' specification. EDX spectra (Figure S2) showed that consortium particles (20 nm) were gold–silver core–shell NPs. As expected, the Au core could not be detected for 110 nm NPs using EDX or high-angle annular dark-field scanning transmission electron microscopy (HAADF-STEM) as it is below the concentration limit for detection, buried in the Ag shell (the manufacturers MSDS state that the Au core is present, confirmed by ICP-MS at NCNHIR (Figures S3 and S4).

The dissolution rates of the four types of AgNPs were examined at both pH 5 and 7 (inorganic buffers) by ICP. The dissolution rates were higher at pH 5 than at pH 7 (Figures S5 and S6). All particles, with the exception of 20 nm citrate-capped particles, displayed less than 1% total release of silver to the solution over a 3-day incubation period (Figures S5 and S6). Our results differ from the previous work of Bouwmeester et al. (2011) using similar particles, where 5–15% dissolution was observed with citrate stabilized particles. These differences are best explained by differences in methodology, dissolution medium and separation techniques used by the different laboratories (Figure S7). The 20-nm citrate-capped particles displayed greater dissolution than the other particles at both pH 5 and 7; >4% Ag was released into the solution after 3 days of incubation (Figure S5). Having established that the particles were relatively stable against dissolution solution, we assessed

their morphology and the effect of surfactant addition by TEM (Figure 1). Regardless of stabilization, or the presence of the model surfactant DPPC, 20 nm AgNPs displayed a greater tendency to aggregate than the 110 nm particles, as expected due to surface energy considerations. Evidence of particle aggregation and significant *coarsening* is also observed for the 20 nm particles with both capping agents (Figure 1C and G). The limited aggregation of 110 nm AgNPs observed in buffer (Figure 1A and E) was completely lost upon addition of DPPC (Figure 1B and F). DPPC also had a dramatic effect on the 20 nm AgNPs with only small clusters of NPs and no coarsening observed (Figure 1D and H).

Acute findings

Histology of the lung 24 h after particle administration demonstrated no significant injury. There was minor consolidation of the tissue and presence of airway thickening with all four types of AgNPs. The most significant consolidation and thickening appeared in PVP-stabilized AgNP-treated mice as well as 110 nm citrate-stabilized AgNP treated mice (Figure 2). Although in general there was minimal peribronchial or perivascular inflammation, there was observable cellular accumulation in the tissue of mice treated with PVP-stabilized AgNP; this accumulation was localized in the 20 nm treatment group, but diffuse in the 110 nm treatment group. Overall, there were no signs of injury or overt inflammation as evidenced by histology.

Cell count and cytology serve as quantitative and qualitative measures of inflammation. As expected with only minor tissue consolidation and airway thickening demonstrated in the histology of the AgNP-treated mice, there was no significant change in BAL cell count (Figure 3) or alterations in the inflammatory cell population (in all conditions macrophages constituted >98% of the BAL cells), or increase in protein content within the BAL, indicating no loss of barrier function (Figure S9). To confirm that there was not significant injury to the lung lining a LDH assay was performed using the BAL; LDH levels were not significantly different between treatment groups (data are not shown). In addition, RT-PCR showed less than a twofold change in mRNA expression of CCL2, IL1B, IL6, CXCL10 and IL12B in the BAL cells from AgNP-treated mice as compared to the control (water) (Figure S8). NOS2 was not detectable in any of the conditions. These markers were chosen as indicators of macrophage activation. Macrophages are the principal phagocytic cells of the lung lining; a key point of interaction with AgNPs, and thus their activation is predicted in the presence of cellular injury. Characterization of the macrophage population by immunohistochemistry demonstrated that there were Cd11b+ cells present in all lung tissues (localized to both peribronchial and perivascular regions). However, this staining was independent of particle treatment (Figure 4). CD11b is a migratory integrin and is often used as a marker of immature or recruited cells. Therefore, this staining indicates that AgNP exposure does not increase inflammatory cell recruitment. As a whole these data indicate that there was no classic inflammatory response to any of the AgNP exposures.

In order to measure the effects of AgNPs on the lung lining fluid composition, both phospholipid content and surfactant protein content were measured. There was no significant increase in phosphate content with AgNP treatment, except within the 20 nm citrate-stabilized particle group (Figure S10). To determine potential protein–particle effects,

immunoblotting for both SP-D and SP-B was performed. There was no significant change in SP-B expression between treatment groups. However, there was a significant *decrease* in SP-D expression in mice treated with PVP-stabilized particles (both 20 and 110 nm Ag); this decrease was greatest in the 110 nm treatment group (Figure 5). These changes in the composition of the lung lining fluid did not alter *in vitro* surface-active function as measured by capillary surfactometry. There were no significant differences between treatment groups for either percent capillary open or initial opening pressure (Figure S11).

Measuring mechanical impedance allows one to determine the frequency dependence of pulmonary resistance and elastance and hence to partition functional characteristics in terms of airway and parenchymal components. Lung mechanical function was assessed by forced oscillation technique and R_L (resistance) and E_L (spectra) were fit to three component models, which have been used previously in assessing lung injury (Groves et al., 2012, 2013; Massa et al., 2014). At PEEP of 3, all particle-treated mice displayed a significant increase in both R_L and E_L spectra as compared to the control, with the exception of the 110 nm citrate-stabilized particle treatment group in which only the elastance spectra were significantly increased (Figure 6A–C). Furthermore, elastance was significantly greater in mice treated with 110 nm PVP-stabilized AgNPs than in mice treated with other types of AgNPs (Figure 6C). The increases seen in the R_L and E_L spectra appear to occur predominantly in the low frequency ends of the spectra (Figure 6D and E), indicating increased tissue resistance and inherent tissue elastance, with little effect on the main conducting airways.

Figure 6(D)–(G) illustrates the parameter estimates from model fits made at PEEP 3. From the model, one can calculate the parameter a/c, which is determined predominantly by low frequency behavior and thus is an estimate of tissue resistance, and the parameter b, which is an estimate of high frequency or airway resistance. Across all levels of PEEP a/c were significantly increased with all types of AgNP administration (Figure 6D). However, b was not significantly altered by particle exposure at any PEEP (Figure 6F). Furthermore, there was no significant alteration to a/c with increasing PEEP, except from PEEP 0 to 1. In contrast, with all treatments, parameter b decreased with increasing PEEP. These findings are consistent with our observation of no significant structural alteration as a result of particle administration.

In parallel with the resistance parameters one can estimate E_0, as a measure of low frequency elastance, and ΔE, as a measure of the frequency-dependent increase in elastance (Figure 6E and G). E_0 was consistently raised by particle administration across PEEP values, although this increase was only statistically significant for 110 nm PVP-stabilized AgNP (PEEPs 1–6 cm H_2O). Similar to the resistance parameters, E_0 responses to increasing PEEP were not altered by particle administration. In contrast, ΔE, which was raised at low PEEP within particle-administered mice (and to the greatest extent within 110 nm PVP-stabilized AgNPs), was completely resolved by increasing the PEEP.

Long-term effects

The most pronounced acute effects occurred within the PVP-stabilized AgNP-treated mice. Therefore, longer-term studies to examine for the persistence of the responses focused on 20

and 110 nm PVP instillations, and mice were examined at 7 and 21 days post-instillation. Similar to the acute profile, there was no significant increase in protein concentration (Figure S9) as compared to control (water), and no injury or loss of structural integrity of tissue as evidenced by histology (data is not shown). In addition, cytospins revealed a monocytic cell population from the BAL. While AgNP-treated mice cell counts were not significantly increased as compared to the controls at 7 and 21 days, there was an increase in total cell count when comparing acute and chronic time points (Figure 3). However, the most significant difference between acute and chronic profiles was demonstrated in the respiratory mechanics. At 7 and 21 days there was no significant difference between 20 nm PVP-stabilized AgNP-treated mice compared to control in either resistance or elastance; all previous tissue stiffnesses seen at 1 day post-instillation had resolved by 7 days (Figure 7B). One hundred and ten nanometer PVP-treated mice displayed significantly lower elastance at 7 days, but was similar to control by 21 days (Figure 7C). Overall, all changes in lung function resolved by 21 days post-instillation.

Discussion

The goal of this study was to determine whether AgNPs, at a dose that does not elicit cellular toxicity, induces organ level toxicological effects. AgNPs are known to produce significant toxic effects when applied to cells *in vitro* (Asharani et al., 2008; Park et al., 2011), although it is unknown whether the same toxic effects are elicited with an *in vivo* approach. The lung is a complex system, with potential for numerous interactions between AgNPs and its components including the lung lining fluid (alveolar cells, proteins, lipids and surfactant). This system complexity and combination of potential interactions cannot be replicated in an *in vitro* system. Therefore, to truly examine the potential consequences of AgNP exposure it is necessary to measure organ level responses following *in vivo* exposure. This study demonstrates that, in the absence of cellular injury, there was an increase in work of breathing as a consequence of AgNP exposure. In addition, we provide evidence of AgNP–lipid and protein interactions as well as changes in BAL composition that correlate with changes in respiratory effort, and may represent a mechanism for these responses.

From the respiratory mechanics data, one can observe that the elastance and resistance spectra do not change in parallel. This, in conjunction with PEEP failing to improve function, is best explained by increased tissue stiffness and heterogeneity, which leads to an increased work of breathing. One explanation for these observations is that particles are distributed unevenly within the lung; reaching some of the lower airways and reducing the airway opening. Both AgNP size and functionalization were significant factors in the extent of the increased work of breathing. There was a significant, acute increase in pulmonary elastance with AgNP administration that was not resolvable by PEEP and was most pronounced with 110 nm PVP-stabilized particles. When examined at 7 and 21 days post-instillation, smaller PVP-stabilized particles demonstrated resolved tissue stiffness by 7 days, while larger PVP-stabilized particles experienced dramatically decreased elastance at 7 days. All changes in work of breathing resolved by 21 days. Therefore in the absence of cellular injury, AgNPs acutely increase the work of breathing possibly via direct interactions with components of the lung lining fluid. The lung lining fluid comprises a complex mixture

of lipids and proteins that regulate both surface tension and innate immunity (Atochina-Vasserman et al., 2009; Dhar et al., 2012).

The lung lining fluid is produced and recycled by the pulmonary epithelium, while alveolar macrophages operate to absorb and degrade lining materials (Andreeva et al., 2007). Loss of regulation of this intricate homeostatic system results from Type II epithelial cell injury or hyperplasia as well as macrophage activation. Both alveolar macrophages and Type II epithelial cells are key points of interaction for nanoparticles within the lung. Type II cells are responsible for the production of both the surface-active components of the lung lining, namely phospholipids and the proteins SP-B and C, and innate immune regulatory elements, such as SP-A&D (Andreeva et al., 2007). Nanoparticle biophysics will affect interactions with components of the lung lining fluid and consequent interactions with alveolar macrophages as well as Type II epithelial cells.

Previous studies have shown that AgNPs interact with phospholipids (Leo et al., 2013) and given the high concentration of phospholipid in the lung lining these molecules represent likely targets for direct interaction. The association of AgNPs with lung lining phospholipids will alter surface active function and particle characteristics. Here, we demonstrate that size and functionalization alter particle aggregation within DPPC (the primary component of lung lining fluid) with larger PVP-stabilized particles being the most readily dispersed in DPPC. These *in vitro* data provide a potential explanation for the respiratory function effects. It is reasonable to propose that by interacting with the phospholipids of the lung lining, AgNPs are capable of reducing surface active function. Thus, as size and functionalization are key components of this interaction, it is reasonable to propose that these particle characteristics will determine *in vivo* outcome. Lipid-capped particles form strands in the presence of SP-B, increasing the surface tension of the lung lining fluid (Tatur & Badia, 2012). Although there was no change in SP-B content of the BAL, this does not preclude alterations in its aggregation status. One might predict a change in capillary surfactometry measurements with particle–lipid interactions. However, this technique is not sensitive to *localized* changes such as appear to occur with nanoparticle administration. The respiratory mechanics (a disproportionate increase in E_L vs. R_L) indicate heterogeneity in the tissue response to particles (Bates & Allen, 2006); indicating localized AgNP interaction with the lung lining. Such localized changes may go undetected when the whole BAL is analyzed.

A second significant component of the lung lining is the pulmonary collectins, including SP-D. These proteins are produced through an alternate secretory pathway to the surface active components and thus by measuring the relative content of SP-B and D one can gain insight into Type II cell function (Atochina-Vasserman et al., 2009). In this study, SP-B levels were unaltered by AgNP exposure, which correlates with a lack of change in the surfactometry assay. However, there was an acute, significant decrease in SP-D concentration in the BAL of mice treated with PVP-stabilized particles, indicating potentially reduced production or increased turnover of the collectins. As both SP-B and SP-D are derived from Type II cells and SP-B levels are unchanged, it seems most likely that this decrease results from increased SP-D turnover by alveolar macrophages, possibly as a result of binding to AgNP (Ruge et al., 2012). SP-D contains a carbohydrate recognition domain, which is predicted to bind

such molecular entities as the PVP functionalization group. Binding to the carbohydrate recognition domain of collectins results in aggregation and targeting toward macrophages and lung clearance (Vuk-Pavlovic et al., 2001). The possibility of such a mechanism is supported by the work of Salvador-Morales et al. (2007) who showed that nanoparticles have the potential to interact with the carbohydrate recognition domain of collectins *in vitro*, depending upon the NP biophysical properties. These acute changes in SP-D content may also have provided a trigger for the observed decrease in elastance at 7 days post-instillation by 110 nm PVP-treated mice. Resolution by 21 days implies restoration of surfactant composition. Importantly, there is no change in SP-D levels 7 and 21 days post-instillation of PVP-stabilized particles.

One reason for the differences in pulmonary function observed between PVP and citrate-stabilized particles may be in their tendency to aggregate and dissolve. In this study, particles were suspended in water for delivery into the lung; and the spectrophotometry confirmed no silver particle aggregation when suspended in water over the course of many minutes, indicating we had achieved a homogeneous suspension during intratracheal delivery. However, once within the high ionic strength environment of the alveolar system, the citrate-stabilized particles are more likely to aggregate and precipitate. Although, our *in vitro* studies indicate that particle size is a more important factor in determining particle aggregation, especially within the context of a lipid environment (Figure 1). Furthermore, although citrate stabilized AgNPs do dissolve faster than PVP-stabilized AgNPs, the loss of Ag^+ within the time frame of this experiment was less than ~4% for any particle. Therefore, it is unlikely that these properties explain the differential functional effects observed with PVP-stabilized AgNPs.

In the event that functionalization of particles results in inefficient clearance from the lung, there is the potential for AgNPs to prevent binding of SPs to receptors on the Type II cells effecting SP production and recycling, leading to more chronic dysfunction. Further studies are required to investigate these possibilities. Importantly, the significant decrease in SP-D content following exposure to PVP-stabilized particles will compromise the effectiveness of the innate immune system if not cleared acutely, leaving the respiratory system more vulnerable to infection (Thacker et al., 2014).

Conclusion

Low dose intratracheal exposure to AgNPs leads to significant changes in the lung lining components and in the mechanical function of the lung; without producing significant cellular injury. Such interactions were dependent upon size and AgNP-stabilization, but resolved over time. These changes may result from AgNP–lung lining fluid interactions including: phospholipid, SPD and alveolar macrophages. Further studies are required to better understand the mechanisms of action; however, from the increased work of breathing in the absence of injury and altered SP-D level, it becomes clear that the toxicology of such particles should be considered at the level of organ physiology in addition to direct cellular injury.

Supplementary Material

Refer to Web version on PubMed Central for supplementary material.

Acknowledgments

Special thanks to Thea Golden, Helen Abramova, Chang Jiang Guo, and Pamela Scott for their support in the laboratory; as well as Don Baer and Joel Pounds at PNNL for useful discussions on particle chemistry.

Declaration of interest

This investigation was supported by the National Institute of Environmental Health Sciences (NIEHS) 1 U19ES019536-01 and the NIH Training in Environmental Toxicology 5T32ES007148. The NIEHS Centers for Nanotechnology Health Implications Research (NCNHIR) was established with the centers funded by RFA ES-09-011. These centers formed a consortium with other NIEHS funded researchers and other federal labs in the area of Nano EHS and worked together on a select set of engineered nanomaterials provided to the consortium by NIEHS. Any opinions, findings, conclusions or recommendations expressed herein are those of the author(s) and do not necessarily reflect the views of the National Institute of Environmental Health Sciences/NIH.

References

Allen G, Bates J. Dynamic mechanical consequences of deep inflation in mice depend on type and degree of lung injury. J Appl Physiol. 2004; 96:293–300. [PubMed: 12949024]

Andreeva AV, Kutuzov MA, Voyno-Yasenetskaya TA. Regulation of surfactant secretion in alveolar type II cells. Am J Respir Cell Mol Biol. 2007; 293:L259–L271.

Asharani PV, Low Kah Mun G, Hande MP, Valiyaveettil S. Cytotoxicity and genotoxicity of silver nanoparticles in human cells. ACS Nano. 2008; 3:279–290. [PubMed: 19236062]

Atochina-Vasserman EN, Gow AJ, Abramova H, Guo CJ, Tomer Y, Preston AM, et al. Immune reconstitution during *Pneumocystis* lung infection: disruption of surfactant component expression and function by S-nitrosylation. J Immunol. 2009; 182:2277–2287. [PubMed: 19201882]

Bakshi MS, Zhao L, Smith R, Possmayer F, Petersen NO. Metal nanoparticle pollutants interfere with pulmonary surfactant function *in vitro*. Biophys J. 2008; 94:855–868. [PubMed: 17890383]

Bates JH, Allen GB. The estimation of lung mechanics parameters in the presence of pathology: a theoretical analysis. Ann Biomed Eng. 2006; 34:384–392. [PubMed: 16468093]

Bligh EG, Dyer WJ. A rapid method of total lipid extraction and purification. Can J Biochem Physiol. 1959; 37:911–917. [PubMed: 13671378]

Bouwmeester H, Poortman J, Peters RJ, Wijma E, Kramer E, Makama S, et al. Characterization of translocation of silver nanoparticles and effects on whole-genome gene expression using an *in vitro* intestinal epithelium coculture model. ACS Nano. 2011; 5:4091–4103. [PubMed: 21480625]

Casey J, Kaplan J, Atochina-Vasserman EN, Gow AJ, Kadire H, Tomer Y, et al. Alveolar surfactant protein D content modulates bleomycin-induced lung injury. Am J Respir Crit Care Med. 2005; 172:869–877. [PubMed: 15994463]

Clement JL, Jarrett PS. Antibacterial silver. Metal-Based Drugs. 1994; 1:467–482. [PubMed: 18476264]

Demokritou P, Gass S, Pyrgiotakis G, Cohen JM, Goldsmith W, Mckinney W, et al. An *in vivo* and *in vitro* toxicological characterisation of realistic nanoscale CeO_2 inhalation exposures. Nanotoxicology. 2013; 7:1338–1350. [PubMed: 23061914]

Dhaliwal K, Scholefield E, Ferenbach D, Gibbons M, Duffin R, Dorward DA, et al. Monocytes control second-phase neutrophil emigration in established lipopolysaccharide-induced murine lung injury. Am J Resp Crit Care. 2012; 186:514–524.

Dhar P, Eck E, Israelachvili J, Lee D, Min Y, Ramachandran A, et al. Lipid–protein interactions alter line tensions and domain size distributions in lung surfactant monolayers. Biophys J. 2012; 102:56–65. [PubMed: 22225798]

Ding N, Kunugita N, Ichinose T, Song Y, Yokoyama M, Arashidani K, Yoshida Y. Intratracheal administration of fullerene nanoparticles activates splenic CD11b+ cells. J Hazard Mater. 2011; 194:324–330. [PubMed: 21872392]

Foldbjerg R, Dang D, Autrup H. Cytotoxicity and genotoxicity of silver nanoparticles in the human lung cancer cell line, A549. Arch Toxicol. 2011; 85:743–750. [PubMed: 20428844]

Groves AM, Gow AJ, Massa CB, Hall L, Laskin JD, Laskin DL. Age-related increases in ozone-induced injury and altered pulmonary mechanics in mice with progressive lung inflammation. Am J Physiol Lung Cell Mol Physiol. 2013; 305:L555–L568. [PubMed: 23997172]

Groves AM, Gow AJ, Massa CB, Laskin JD, Laskin DL. Prolonged injury and altered lung function after ozone inhalation in mice with chronic lung inflammation. Am J Respir Cell Mol Biol. 2012; 47:776–783. [PubMed: 22878412]

Leo BF, Chen S, Kyo Y, Herpoldt KL, Terrill NJ, Dunlop IE, et al. The stability of silver nanoparticles in a model of pulmonary surfactant. Environ Sci Technol. 2013; 47:11232–11240. [PubMed: 23988335]

Massa CB, Scott P, Abramova E, Gardner C, Laskin DL, Gow AJ. Acute chlorine gas exposure produces transient inflammation and a progressive alteration in surfactant composition with accompanying mechanical dysfunction. Toxicol Appl Pharmacol. 2014; 278:53–64. [PubMed: 24582687]

Moriya H, Moraes J, Bates J. Nonlinear and frequency-dependent mechanical behavior of the mouse respiratory system. Ann Biomed Eng. 2003; 31:318–326. [PubMed: 12680729]

Mu Q, Jiang G, Chen L, Zhou H, Fourches D, Tropsha A, Yan B. Chemical basis of interactions between engineered nanoparticles and biological systems. Chem Rev. 2014; 114:7740–7781. [PubMed: 24927254]

Park MVDZ, Neigh AM, Vermeulen JP, De La Fonteyne LJJ, Verharen HW, Briedé JJ, et al. The effect of particle size on the cytotoxicity, inflammation, developmental toxicity and genotoxicity of silver nanoparticles. Biomaterials. 2011; 32:9810–9817. [PubMed: 21944826]

Ruge CA, Schaefer UF, Herrmann J, Kirch J, Canadas O, Echaide M, et al. The interplay of lung surfactant proteins and lipids assimilates the macrophage clearance of nanoparticles. PLoS One. 2012; 7:e40775. [PubMed: 22802970]

Salvador-Morales C, Townsend P, Flahaut E, Vénien-Bryan C, Vlandas A, Green MLH, Sim RB. Binding of pulmonary surfactant proteins to carbon nanotubes; potential for damage to lung immune defense mechanisms. Carbon. 2007; 45:607–617.

Sarkar S, Song Y, Sarkar S, Kipen H, Laumbach R, Zhang J, et al. Suppression of the NF-kB pathway by diesel exhaust particles impairs human antimycobacterial immunity. J Immunol. 2012; 188:2778–2793. [PubMed: 22345648]

Shang L, Nienhaus K, Nienhaus GU. Engineered nanoparticles interacting with cells: size matters. J Nanobiotechnol. 2014; 12:5.

Shim KI, Lee YI, Lee KJ, Joung J. An organometallic route to highly monodispersed silver nanoparticles and their application to inkjet printing. Mater Chem Phys. 2008; 110:316–321.

Tatur S, Badia A. Influence of hydrophobic alkylated gold nanoparticles on the phase behavior of monolayers of DPPC and clinical lung surfactant. Langmuir. 2012; 28:628–639. [PubMed: 22118426]

Tejamaya M, Romer I, Merrifield R, Lead J. Stability of citrate, PVP, and PEG coated silver nanoparticles in ecotoxicology media. Environ Sci Technol. 2012; 46:7011–7017. [PubMed: 22432856]

Thacker S, Moran A, Lionakis M, Mastrangelo M, Halder T, Huby MDP, et al. Restoration of lung surfactant protein D by IL-6 protects against secondary pneumonia following hemorrhagic shock. J Infect. 2014; 68:231–241. [PubMed: 24291043]

Tolaymat TM, El Badawy AM, Genaidy A, Scheckel KG, Luxton TP, Suidan M. An evidence-based environmental perspective of manufactured silver nanoparticle in syntheses and applications: a systematic review and critical appraisal of peer-reviewed scientific papers. Sci Total Environ. 2010; 408:999–1006. [PubMed: 19945151]

Vuk-Pavlovic Z, Standing JE, Crouch EC, Limper AH. Carbohydrate recognition domain of surfactant protein d mediates interactions with Pneumocystis carinii glycoprotein A. Am J Respir Cell Mol Biol. 2001; 24:475–484. [PubMed: 11306442]

Warheit DB, Reed KL, Delorme MP. Embracing a weightof-evidence approach for establishing NOAELs for nanoparticle inhalation toxicity studies. Toxicol Pathol. 2013; 41:387–394. [PubMed: 23242579]

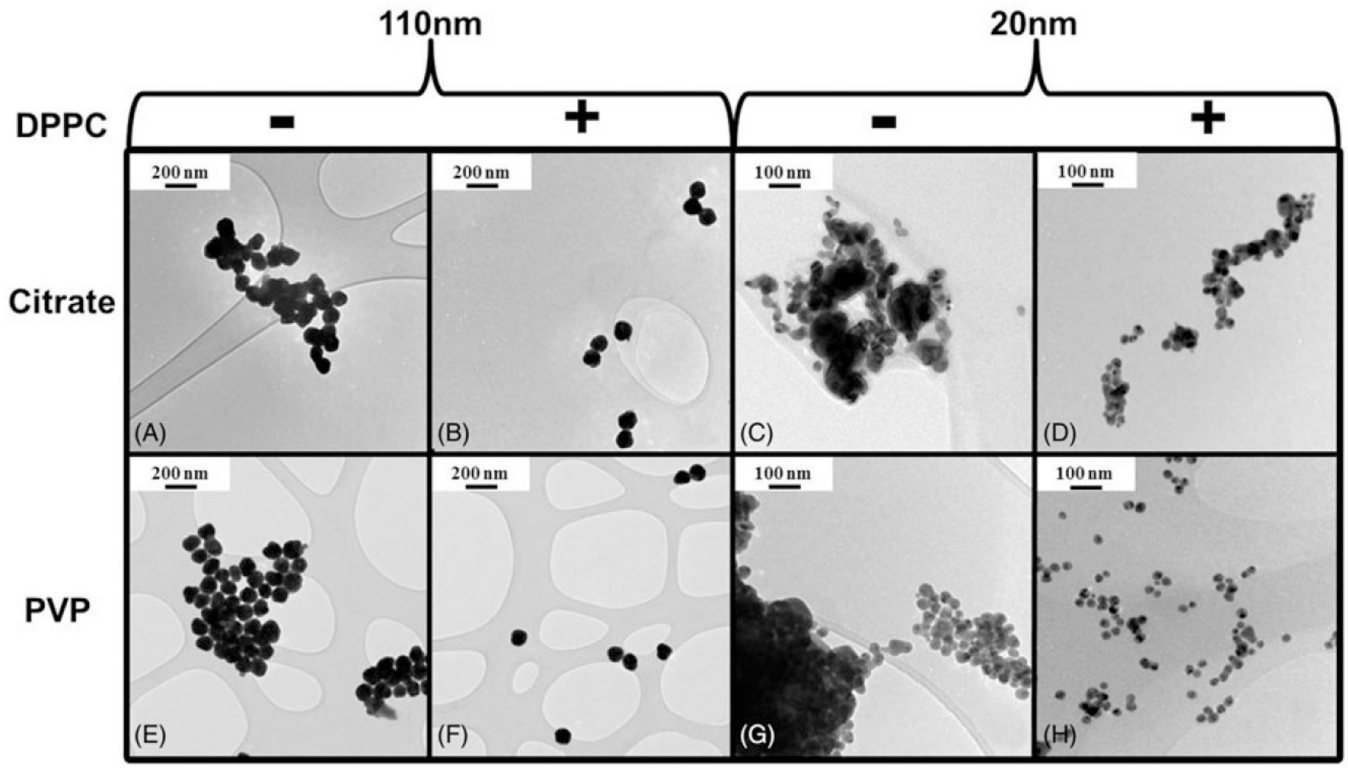

Figure 1.

AgNP morphology and the effect of surfactant addition by transmission electron microscopy: TEM images of citrate versus PVP stabilized AgNPs (20 and 110 nm) incubated in pH 5 solution with and without DPPC at 37 °C for 24 h (magnification at 20×). Addition of DPPC decreased particle aggregation in all instances; however, size was the predominant factor in particle aggregation.

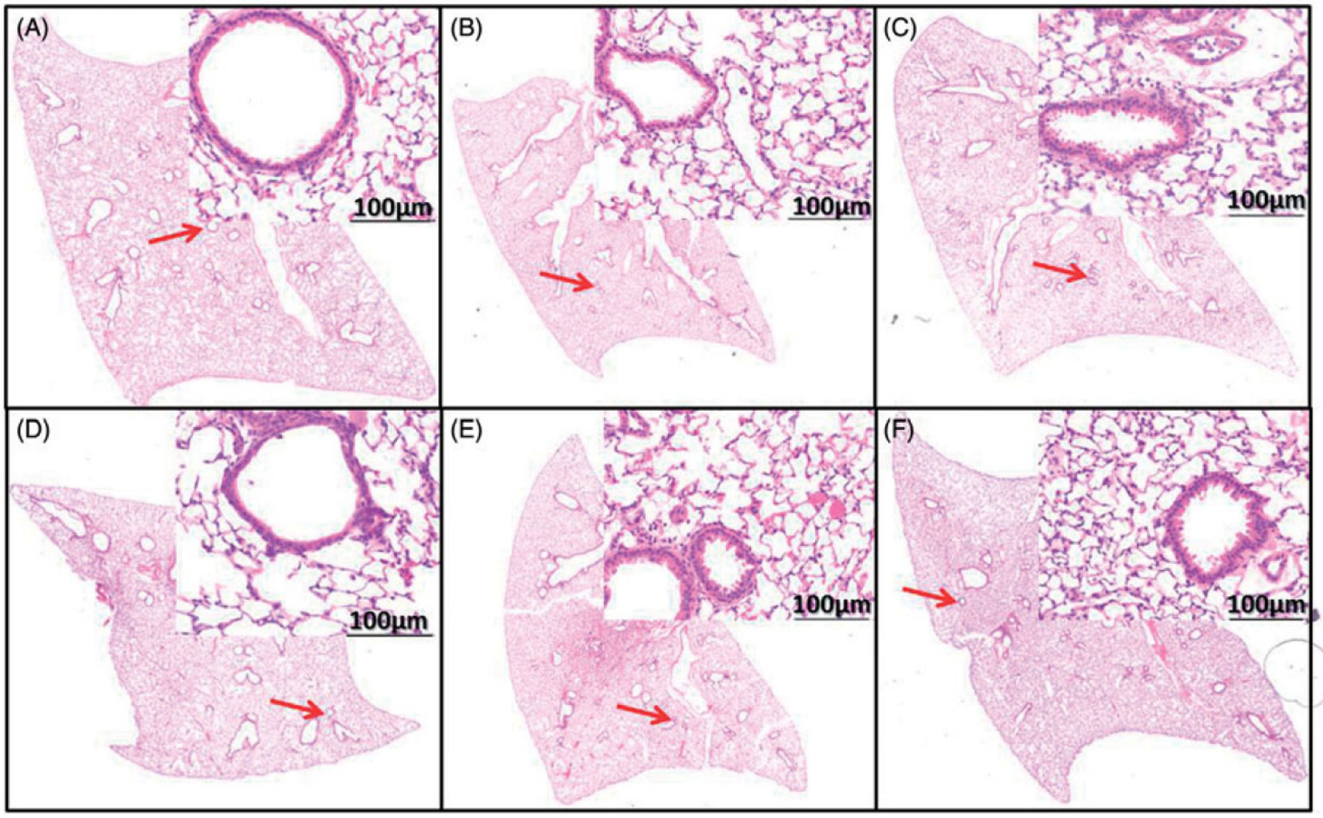

Figure 2.

Lung histology (H&E): Post-mechanical ventilation at 1 day post-instillation, the left lung of the treated mice was inflation fixed, paraffin embedded, sectioned and stained with H&E (whole lung image 0.8×, enlarged image 20×; arrow marks site of interest). (A) Untreated wild-type male mouse, (B) 20 nm citrate-stabilized AgNP treatment, (C) 110 nm citrate-stabilized AgNP treatment, (D) water (control) treatment, (E) 20 nm PVP-stabilized AgNP treatment, (F) 110 nm PVP-stabilized AgNP treatment; all AgNP-treated mice displayed slight tissue consolidation and airway thickening. This was most pronounced with 110 nm citrate and both PVP-stabilized AgNP treated mice. But overall lung structure for all treatments was normal with no indication of overt inflammation.

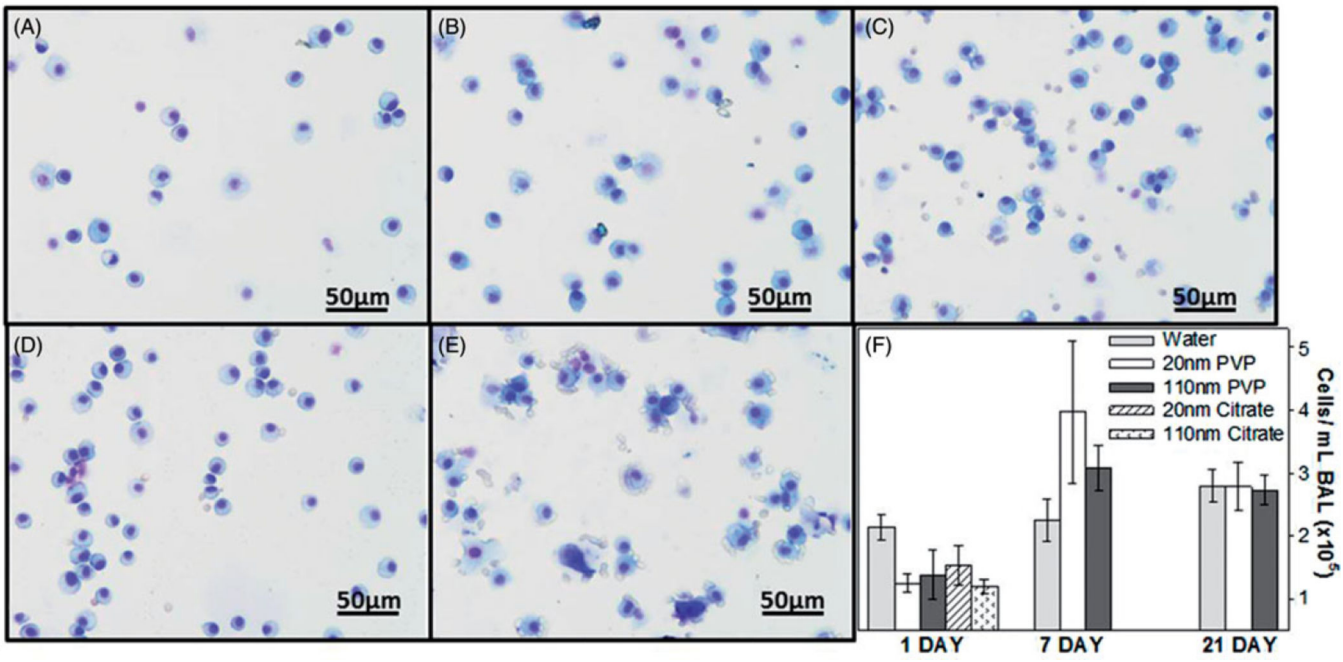

Figure 3.

Cell count and cytology using BALF: cell counts (mean ± standard error ($\times 10^5$)) were normalized to 1 mL BALF and ~30 000 cells were used for cytology. (A) Water (control) treatment displayed slightly elevated cell count, but no sign of neutrophilia, (B) 20 nm citrate-stabilized AgNP treatment, (C) 110 nm citrate-stabilized AgNP treatment, (D) 20 nm PVP-stabilized AgNP treatment, (E) 110 nm PVP-stabilized AgNP treatment (A–E all 1 day post-instillation); all AgNP-treated mice displayed acute, decreased cell count as compared to the control with no signs of neutrophilia, but all treatments were within normal cell count range. The dominant cell type was macrophages in all treatments, neutrophils and lymphocytes <1% of cell population. The bar graph displays the cell count time course (n = 4 for all treatment groups/time points).

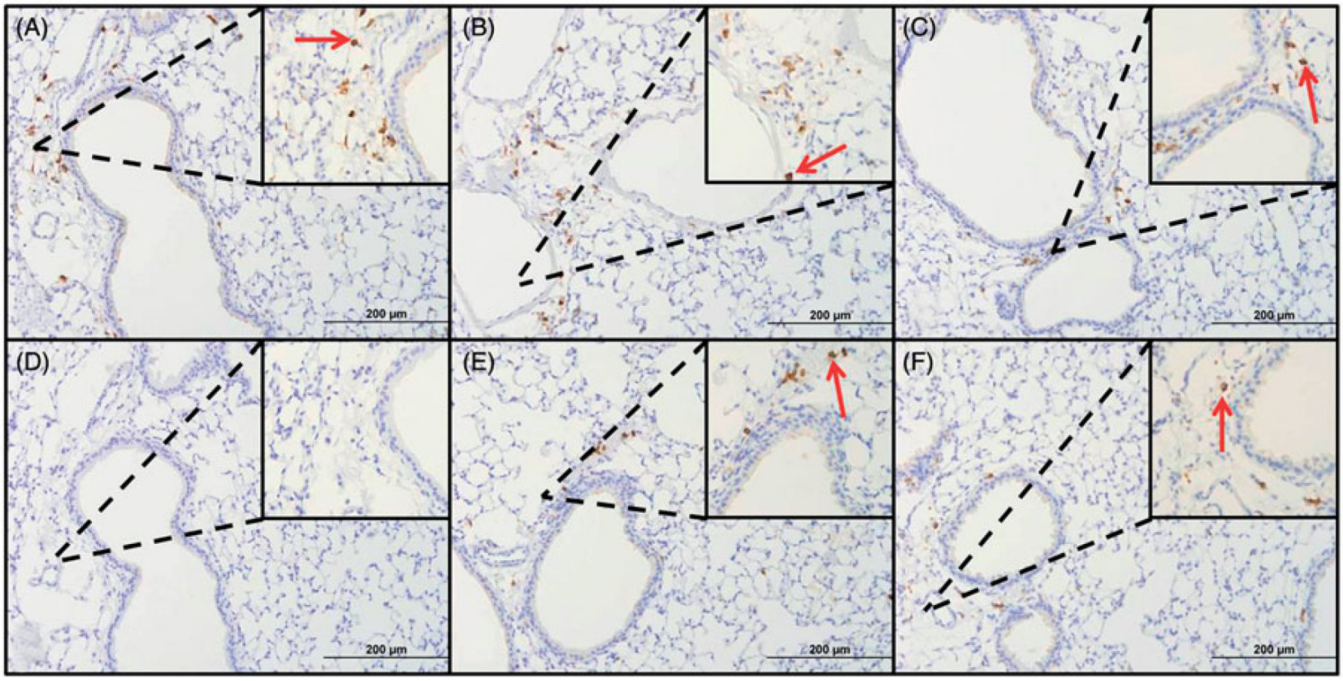

Figure 4.

Immunohistochemistry: Lung tissue from 1 day post-instillation was stained with anti-Cd11b to assess cell recruitment (main image −20×, enlarged image −40×; arrows indicate Cd11b+ cells). (A) Water (control) treatment, (B) 20 nm citrate-stabilized AgNP treatment, (C) 110 nm citrate-stabilized AgNP treatment, (D) IgG control using tissue from water treatment, (E) 20 nm PVP-stabilized AgNP treatment, (F) 110 nm PVP-stabilized AgNP treatment. The staining is isolated to peribronchial and perivascular sections of the lung. Positive staining is independent of AgNP treatment.

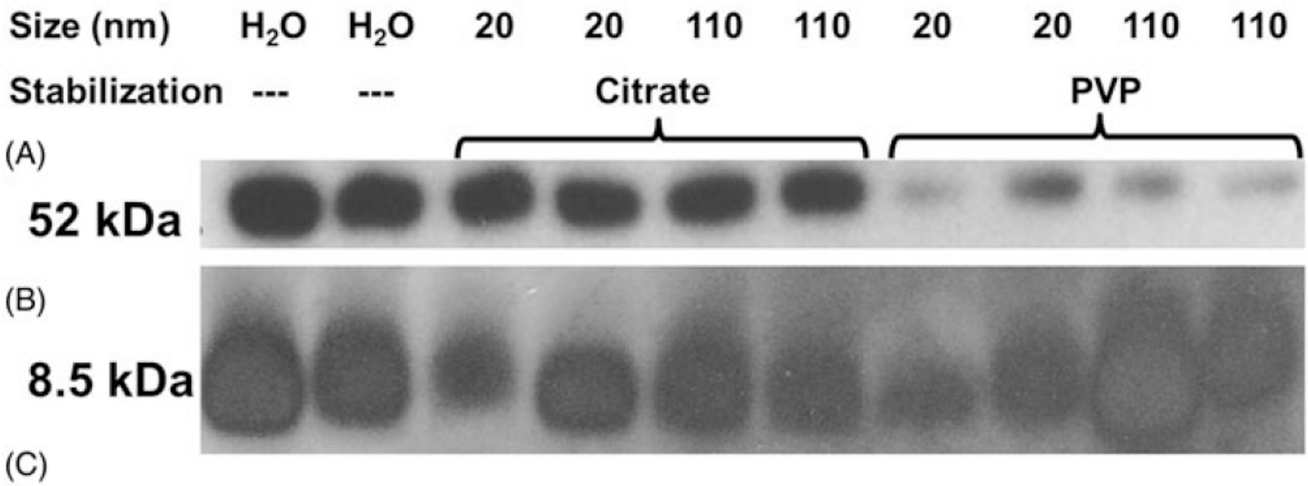

Treatment	SP-D/SP-B ratio compared to control	SP-D content compared to control	SP-B content compared to control
Water	1.00 +/- 0.091	1.00 +/- 0.072	1.00 +/- 0.026
20nm Citrate	0.900 +/- 0.096	0.936 +/- 0.063	1.05 +/- 0.050
110nm Citrate	0.902 +/- 0.072	0.944 +/- 0.036	1.05 +/- 0.047
20nm PVP	0.726 +/- 0.065	0.754 +/- 0.052*	1.04 +/- 0.043
110nm PVP	0.637 +/- 0.027*	0.661 +/- 0.028*†	1.04 +/- 0.053

Figure 5.

Surfactant expression via immunoblotting: 1 day-post intratracheal instillation. (A) SP-D immunoblot (B) SP-B immunoblot (c) SP-D/SP-B ratios; SP-D expression decreases significantly when lungs are treated with PVP-stabilized particles, while SP-B expression is not significantly altered with particle exposure as compared to the control. Therefore, the SP-D/SP-B ratio decreases with PVP-stabilized particle exposure (*p<0.05 compared to the control, †p<0.05 compared to citrate-stabilized AgNP treatments; n = 4 for all treatment groups).

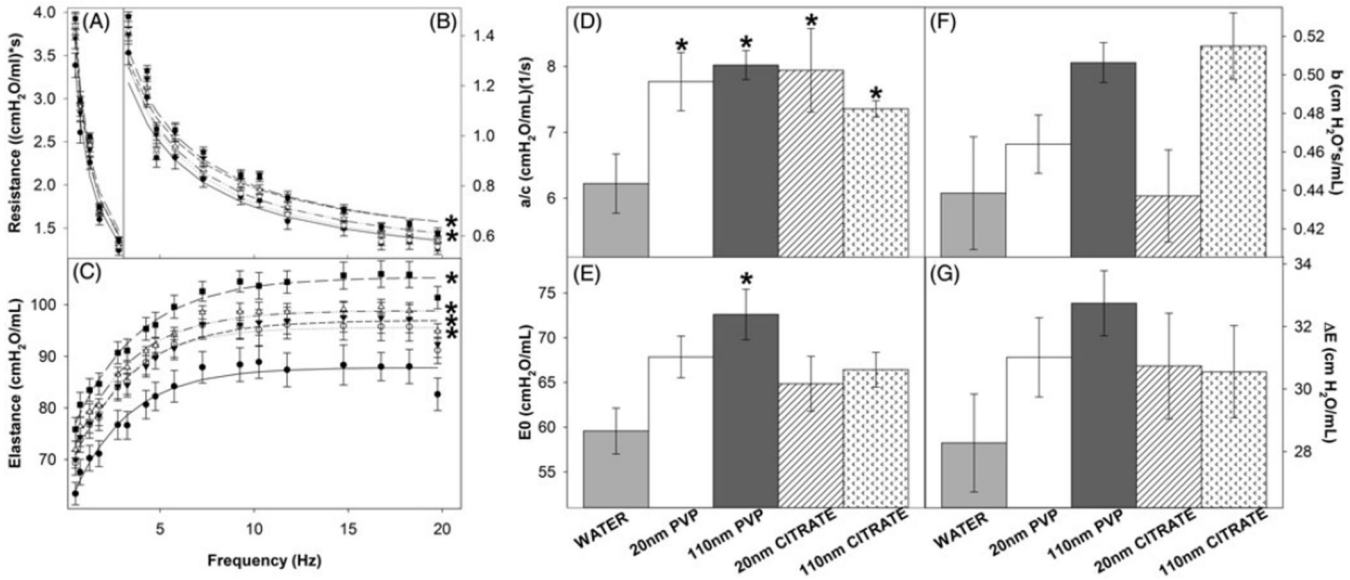

Figure 6.

Resistance (RL) and elastance (EL) spectra using forced oscillation technique: Analysis of impedance measurements at PEEP 3 – 1 day post-intratracheal instillation (A and B) 20 nm AgNP citrate and PVP-stabilized particle as well as 110 nm AgNP PVP-stabilized particle-treated mice were significantly different from the control RL spectra but (C) all AgNP-treated mice were significantly different from the control EL spectra (*p<0.05 compared to the control) (●/solid line = water/model fit; ○/dotted line = 20 nm citrate/model fit; ▼/short dashed line = 110 nm citrate/model fit; ▽/dashed and dotted line = 20 nm PVP/model fit; ■/ long dashed line = 110 nm PVP/model fit), (D) low frequency resistance (a/c), (E) low frequency elastance (E_0), (F) high frequency resistance (b) and (G) magnitude of change in elastance (ΔE) were not PEEP dependent. Isolating the model parameters revealed that the greatest differences occur in the low frequency end of the spectra.

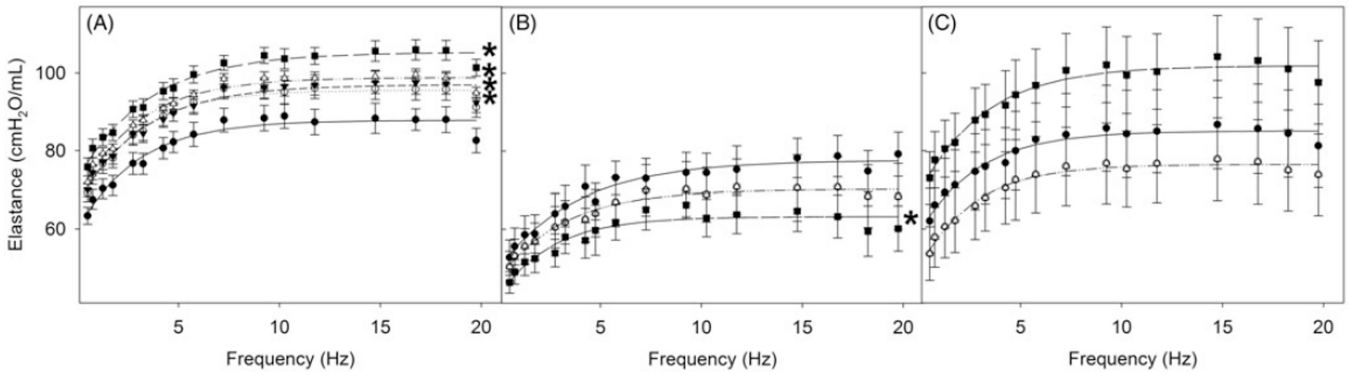

Figure 7.

Elastance (EL) spectra – all time points: Analysis of impedance measurements at PEEP 3 (A) 1 day, all AgNP-treated mice demonstrated significantly increased elastance as compared to control (water), (B) 7 days, acute tissue stiffness documented in 20 nm PVP-stabilized AgNP-treated mice resolves, 110 nm group demonstrates significantly decreased elastance compared to control (C) 21 days, AgNP mice are similar to control (*$p < 0.05$ compared to the control) (●/solid line = water/model fit; ○/dotted line = 20 nm citrate/model fit; ▼/short dashed line = 110 nm citrate/model fit; ▽/dashed and dotted line = 20 nm PVP/model fit; ■/long dashed line = 110 nm PVP/model fit) groups (1 day post-instillation data only).